J Mater Sci: Mater Electron (2016) 27:6413–6418
DOI 10.1007/s10854-016-4579-1

CrossMark

Effect of annealing temperature on the structural, optical and electrical properties of ZnO thin films grown chemically on PS substrate

R. Shabannia[1]

Received: 7 December 2015 / Accepted: 23 February 2016 / Published online: 23 March 2016
© Springer Science+Business Media New York 2016

Abstract ZnO thin films were successfully produced on porous silicon (PS) substrates by a chemical bath deposition method. ZnO thin films were then annealed at 300, 500, and 700 °C for 20 min in nitrogen (N_2) atmosphere. X-ray diffraction, field emission scanning electron microscopy (FESEM), and photoluminescence (PL) were utilized to investigate the effect of post-annealing temperature on the structural, optical, and electrical properties of ZnO thin films. The lattice constant, full width at half maximum, and strain (the grain size) of (0 0 2) peak of ZnO thin films decreased (increased) with increasing the annealing temperature, respectively. The FESEM images revealed that the ZnO thin films are compact array ZnO nanocolumns and were perpendicularly grown to the PS substrate. The biggest ratio of the PL intensity of UV emission to that of visible emission is observed from ZnO thin films annealed at 500 °C. The PL results of the ZnO thin films exhibit that the UV peak positions shift slightly toward lower wavelengths with increase of the annealing temperature. The current–voltage measurements demonstrate that the current level increases as the annealing temperature increases to 500 °C, and then decreases when the temperature further increases up to 700 °C.

1 Introduction

ZnO nanostructures is a semiconductor with extraordinary optical, electronic, and chemical properties that have attracted increasing attention for a great variety of potential applications in devices such as solar cells, gas sensor, light-emitting diodes, UV photodetectors, and etc. [1–7]. A detailed understanding of electrical and optical properties of ZnO nanostructures is essential for use of ZnO nanostructures in the optoelectronics industry because of the carrier relaxation processes strongly affect optoelectronic and electronic characteristics of ZnO nanostructures. The structural and surface morphology of substrates and their lattice mismatch with ZnO nanostructures are significant parameters because these factors control the nature and morphology of fabricated ZnO nanostructures. ZnO nanostructures grown on Si-based substrates have been attracted significant interests in the past few decades because silicon substrate is a stable and high temperature resistant material and a very popular substrate in IC technology [8, 9]. However, it is difficult to directly grow or deposit high quality ZnO nanostructures on silicon substrates, because there is a large stress between ZnO and Si substrate due to the mismatch in their thermal expansion coefficients and lattice constants [10]. Therefore, it is necessary to look for a better substrate for growing high quality ZnO nanostructure. Among porous semiconductors, porous silicon has opened new possibilities for Si-based integrated circuits due to its remarkable optical and electronic properties. It has been used for various adsorptive substances because of its low cost, large internal surface-to-volume ratio, sponge-like structure, adjustable roughness, and strong absorbability. Moreover, PS prepared by the silicon is compatible with silicon IC technology, which provides a possibility to integrate PS-based optical devices [11]. The porous silicon (PS) layer reduces the large mismatches in the lattice constants and thermal expansion coefficients between the ZnO and Si substrates, which also reduces the large stress between the ZnO nanostructures and Si substrate [12]. So for, the ZnO thin films have been

✉ R. Shabannia
rezash56rami@gmail.com

[1] Department of Physics, College of Science, Babol University of Technology, Babol, Iran

widely fabricated by numerous techniques [13–17] but chemical bath deposition (CBD) technique is one of the appropriate chemical synthesis to produce ZnO thin films on various substrates because of its low temperature, non-requirement of sophisticated instruments, simplicity, capability for large-scale production, and affordability. Unfortunately, it is well known that ZnO thin films grown at a relatively low temperature usually showed poor crystallization and optical properties due to its low growth temperature. However, post-annealing of ZnO thin films may provide an efficient technique to reduce the defects and improve the crystalline quality and the optical properties of ZnO thin films [18]. Furthermore, the large lattice mismatch and the large difference in the thermal expansion coefficients between the ZnO thin films and the Si substrates would cause imperfections in the ZnO thin films. To solve this problem, the widely known effective technique of post-annealing treatment can be implemented.

Cui et al. [19, 20] studied effect of annealing temperature and annealing atmosphere on the structure and optical properties of ZnO thin films grown on sapphire (0 0 0 1) substrates by magnetron sputtering and sol–gel method, respectively. Zhu et al. [21] reported on the effect of annealing temperature on the microstructure and optical properties of the ZnO thin films deposited on glass substrates at room temperature by pulsed laser deposition. Gug et al. [22] systematically studied the effect of post-annealing temperature on the properties of ZnO nanorods on Si substrates by using the hydrothermal method. According to Lim et al. [23], the optical properties of ZnO thin film are more dependent on the annealing conditions than on the growing techniques. Cui et al. [20] suggested that annealing atmosphere of N_2 is the most suitable annealing condition for obtaining high quality ZnO thin films with good luminescence performance. To the best of my knowledge, this research is the first to examine the effect of the post-annealing temperature on ZnO thin films synthesized on PS substrate by CBD technique supplemented with oven heating. The oven provided a homogenous temperature distribution for the reaction vessels. Furthermore, in this research, the XRD, FESEM, and PL spectroscopy utilized to study the effect of annealing temperature on the structural, optical, and electrical properties of fabricated ZnO thin films on PS substrates.

2 Experimental details

The porous structure was formed on an n-type Si (100) substrate using the photo electrochemical etching method. The photo electrochemical etching process was carried out in a Teflon cell containing a mixture of hydrofluoric acid and 96 % ethanol with a volume ratio of 1:4. The PS layer was formed with a constant current density of 20 mA/cm^2 for 5 min at room temperature using the Pt wire and Si as cathode and anode, respectively. The sample was illuminated with a 60 W visible lamp during the etching process. The prepared PS substrates were rinsed with deionized (DI) water. A radio frequency (RF) magnetron sputtering system with a sputtering power of 150 W and an argon pressure of 15 mTorr was used to create a ZnO seed layer on the PS substrates. A 170 nm ZnO seed layer was fabricated on the PS substrates. Finally, the ZnO thin films were fabricated on PS substrates by CBD method. First, a 0.050 M/L of zinc nitrate hexahydrate $Zn(NO_3)_2{\cdot}6H_2O$ and an equal molar concentration of hexamethylenetetramine $C_6H_{12}N_4$ were dissolved in DI water at 80 °C separately. The two solutions were combined and the samples vertically placed in a beaker. For growth ZnO thin films, the beaker was placed in an oven for 5 h at 95 °C. Then, the samples were rinsed with DI water and were dried with nitrogen (N_2) gas. In order to study the influence of post-annealing temperature on structural and optical properties of fabricated ZnO thin films, the samples were then annealed for 20 min under the temperatures of 300, 500, and 700 °C in a conventional tube furnace with N_2 atmosphere. After annealing, the fabricated ZnO thin films were naturally cooled down to the room temperature.

The crystal structure of the ZnO thin films was determined by XRD (PANalytical X'Pert PRO MRD PW3040). The morphology of fabricated ZnO thin films was obtained via FESEM (model FEI/Nova NanoSEM 450). The room temperature PL spectrum of the ZnO thin films was analyzed using a photoluminescence spectroscopy system (Jobin–Yvon HR 800 UV, Edison, NJ, USA) with a He–Cd laser with an excitation wavelength and an illumination intensity of 325 nm and 20 mW, respectively. The current–voltage characteristics of the ZnO thin films were performed with increasing step of applied voltage 0.01 V within the voltage range from −5.0 to +5.0 V by using a computer-controlled integrated source meter (Keithley 2400) at room temperature.

3 Results and discussion

An X-ray diffraction experiment was carried out to determine the crystalline orientation and to investigate the effect of post-annealing temperature on the crystallinity of fabricated ZnO thin films. Figure 1 demonstrated the XRD patterns of the as-grown ZnO thin film and annealed ZnO thin films at 300, 500, and 700 °C, respectively. For all the ZnO thin films, a strong diffraction peak (0 0 2) with polycrystalline hexagonal wurtzite crystal structure (the standard data for ZnO; ICSD 01-074-0534) are only observed, indicating that the preferred orientation owing to the lowest surface free energy is along the c-axis perpendicular to PS substrate [24]. The XRD peak position, full width at half maximum (FWHM), lattice constant (c),

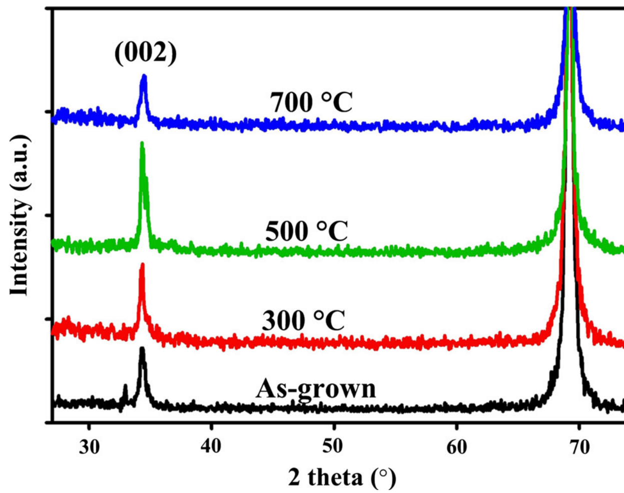

Fig. 1 Typical XRD patterns of ZnO thin films grown on PS substrate; as-grown and annealed under the temperatures of 300, 500, and 700 °C

stress, grain size, and degree of orientation of the ZnO (002) planes for all samples are summarized in Table 1. The (0 0 2) peak position of ZnO thin film shifts to a little higher 2θ angles from 34.375° to 34.475° after annealing, which is possibly owing to the release of intrinsic strain through annealing [25, 26]. As shown in Fig. 1, a weak diffraction intensity (0 0 2) peak is observed for as-grown ZnO thin films and the diffraction intensity (0 0 2) peak obviously increases with the annealing temperature increasing and reaches to the maximum at 500 °C, after that it decreased at 700 °C.

The FWHM and lattice constant (c) of (0 0 2) peak of ZnO thin films decreased with increasing the annealing temperature, as shown in Table 1. The total stress of ZnO thin film originates from extrinsic and intrinsic stresses. The extrinsic stress is mainly associated with thermal expansion coefficient mismatch and lattice mismatch between the ZnO thin film and substrate, while the intrinsic stress is related to defects and impurities. XRD is often used to calculate the residual stress of ZnO thin films compared with other methods (such as Raman, and the technique of curvature measurement) because the strain can be calculated directly by using Bragg's equation. The residual stress σ in the plane of as-grown and post-annealed ZnO thin films can be determined using the following expression [26, 27]:

$$\sigma = \frac{2C_{13}^2 - C_{33}(C_{11} + C_{12})}{2C_{13}} \times \frac{c - c_0}{c_0} \quad (1)$$

where c is the lattice constants of the ZnO thin films obtained from the XRD data, c_0 (5.2066 Å) is the standard lattice constant for unstrained ZnO (ICSD 01-074-0534), and C_{ij} are the elastic stiffness constants of ZnO, i.e., $C_{11} = 207.0$ GPa, $C_{33} = 209.5$ GPa, $C_{12} = 117.7$ GPa and $C_{13} = 106.1$ GPa. The calculated stress of as-grown and annealed ZnO thin films at different temperatures in N_2 are given in Table 1. The negative and positive sign of stress indicate the stresses are compressive and tensile, respectively. The as-grown ZnO thin film and annealed ZnO thin film of 300 °C exhibit a compressive residual stress of −0.2717 GPa. With increasing annealing temperature, eventually exceeds the built-in compressive stress and leads to a change in the direction of stress and reaches the minimum tensile stress of 0.0322 GPa at 500 °C, and then increases to 0.4447 GPa at 700 °C [28].

The grain size of the ZnO thin films along the (002) peak is obtained by the following Scherrer equation [29]:

$$D = \frac{0.9\lambda}{\beta \cos\theta} \quad (2)$$

where D, θ, λ, and β represent the average crystallite size, Bragg diffraction angle, X-ray radiation wavelength, and FWHM value, respectively. The calculated grain size for all samples is given in Table 1. The grain size of the ZnO thin films gradually increased from 25.5 to 36.9 nm with increasing the post-annealing temperature.

The degree of orientation of the (002) plane of the ZnO thin films for all samples were calculated using the following Lotgering relation of [30]:

$$F(hkl) = \frac{P(hkl) - P_0(hkl)}{1 - P_0(hkl)} \quad (3)$$

where $F(hkl)$ is the degree of (hkl) orientation, $P(hkl) = I(hkl)/\sum I(hkl)$ and $P_0(hkl) = I_0(hkl)/\sum I_0(hkl)$. Here $I(hkl)$ is the (hkl) peak intensity and $\sum I(hkl)$ is the sum of the intensities of all peaks in the ZnO thin films' diffraction data. $I_0(hkl)$ is the (hkl) peak intensity and $\sum I_0(hkl)$ is the sum of the intensities of diffraction peaks in the reference

Table 1 Summarized data from XRD patterns of ZnO thin films

Annealing temperature (°C)	(002) peak position (°)	FWHM of (0 0 2) peak	c (Å)	Stress (GPa)	Grain size (nm)	Degree of (002) orientation
As-grown	34.375	0.65	5.2132	−0.2717	25.5	0.50
300	34.375	0.57	5.2132	−0.2717	27.8	0.59
500	34.425	0.53	5.2058	0.0322	30.3	0.79
700	34.475	0.45	5.1958	0.4447	36.9	0.49

data (ICSD 01-074-0534). The calculated values of orientation degree of the (002) plane for all samples is given in Table 1.

The increase of (0 0 2) peak intensity and grain size and decrease of FWHM values demonstrate that the increase of annealing temperature from 300 to 500 °C enhanced the crystal quality of ZnO thin films. This result can be possibly attributed to the two reasons: at first, annealing increases atomic mobility, enhancing the ability of atoms to find the most energetically favored sites. At second, with the increase of the annealing temperature, the densities of the crystallographic defects including dislocations, interstitials and vacancies in ZnO thin films decrease rapidly. These two reasons can lead to yield the best structural property of ZnO thin films annealed at 500 °C in N_2 [31].

Figure 2 shows the cross section FESEM images of the as-grown ZnO thin film and the ZnO thin film after post-annealing temperature of 700 °C for 30 min in N_2 atmosphere. The typical FESEM image exhibits that the fabricated ZnO thin films are compact array ZnO nanocolumns. Figure 2 indicates that the aligned ZnO nanocolumns were grown with high density and perpendicular to the PS substrate. In addition, Fig. 2a, b exhibited that the as-grown and annealed ZnO nanocolumns uniformly distributed over the entire PS substrate and had a length of approximately 230 and 240 nm, respectively. The small pores were formed on the surfaces of the ZnO nanocolumns after post-annealing process, as shown in the inset of Fig. 2b. The origin of the pores within ZnO nanocolumns can be possibly attributed to desorption of zinc and oxygen at defect sites. Generally, ZnO nanostructures fabricated by using a chemical bath deposition method have a larger number of defect sites, such as point defects, and non-stoichiometry [32]. The defect sites will move in the ZnO during the post-annealing process, and desorption will occur on the surface of ZnO nanostructures. Thus, the structural properties of ZnO nanostructures can be affected by changing the morphology and the stoichiometric ratio of the material. In addition, Wang et al. [33] and Lee et al. [34] reported that pore was formed on the surfaces of ZnO nanorods because of the post-annealing process.

PL measurements were carried out at room temperature to study the effect of the post-annealing on the optical properties of ZnO thin films grown on PS substrates. Figure 3 displayed that the as-grown ZnO thin film had weak UV emission at UV region and a strong deep level broad emission band at visible region. While those of samples annealed at 300, 500, and 700 °C for 20 min in N_2 atmosphere had strong UV emission at UV region and a weak deep level broad emission band at visible region. The UV emission band was attributed to a near band edge transition of ZnO, namely, the recombination of the free excitons (376 nm). The exact energy position of UV peak depends on the contribution between the free exciton and the

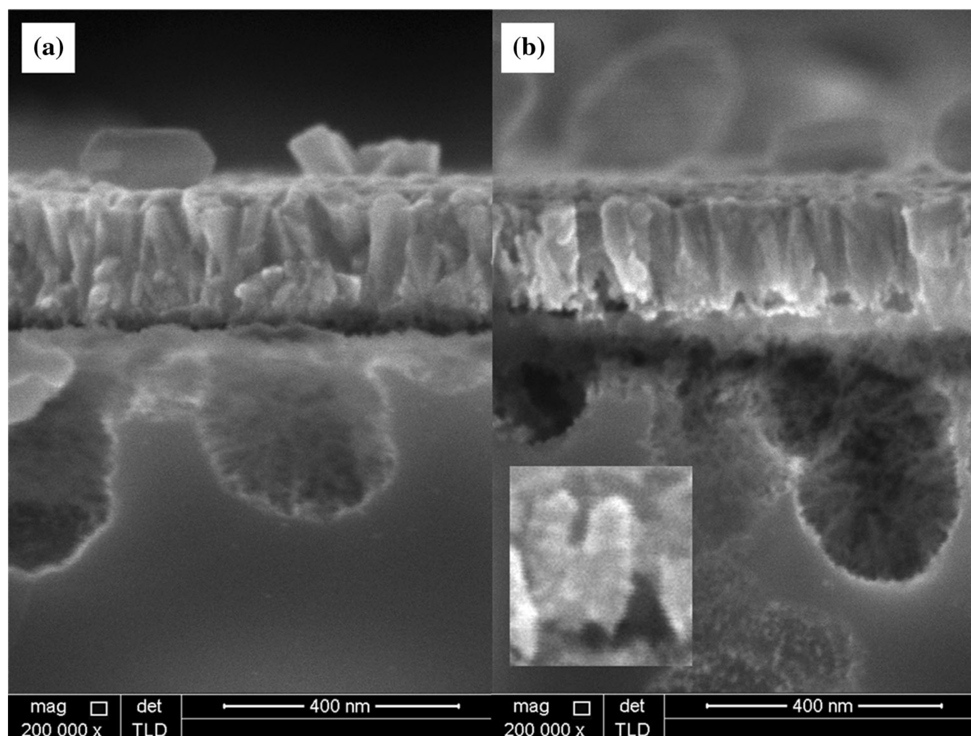

Fig. 2 FESEM images of typical cross section FESEM images of **a** the as-grown ZnO thin film and **b** the ZnO thin film after post-annealing temperatures of 700 °C

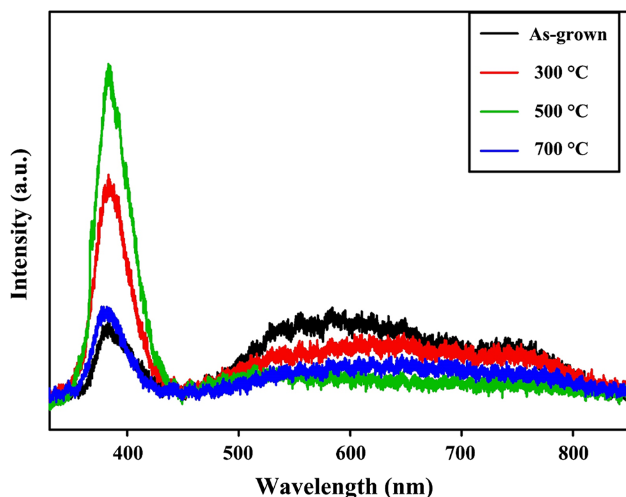

Fig. 3 Room temperature PL spectra of ZnO thin films grown on PS substrate; as-grown and annealed under the temperatures of 300, 500, and 700 °C

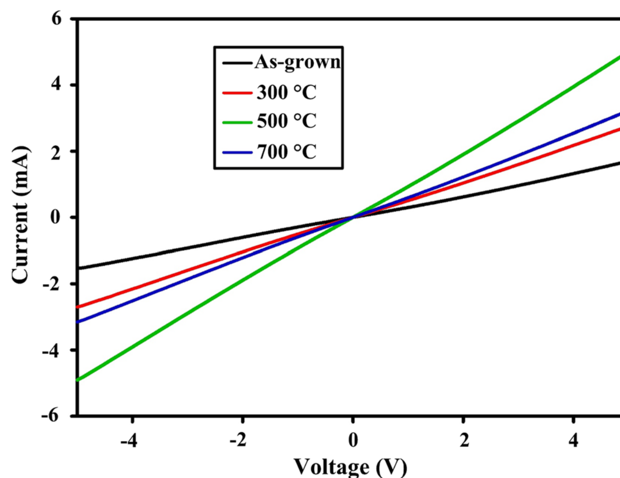

Fig. 4 The current–voltage characteristics of as-grown and annealed ZnO thin films

transition between free electrons to acceptor bound holes [35, 36]. The deep level emission band was related to several defects in the crystal structure of ZnO such as oxygen and zinc vacancies [37, 38], oxygen and zinc interstitials [39], as well as extrinsic impurities [40].

Figure 3 demonstrates that the UV emission intensity of ZnO thin films increased with increased annealing temperature up to 500 °C and then decreased with further increased annealing temperature. The surfaces of ZnO nanostructures synthesized by CBD method were prone to absorb various kinds of functional groups includes elements such as carbon, nitrogen, and hydrogen [41]. These functional groups affect a negative effect on the optical properties of ZnO nanostructures. When the annealing temperature is increased from 300 to 500 °C, the functional group elements were released from the surfaces of ZnO nanocolumn films; as a result, the UV emission intensity is strongly enhanced. During the thermal treatment process at higher annealing temperature of 700 °C, the concentration of defects such as oxygen and zinc vacancies also increased due to the thermal diffusion process, resulting in that the ZnO nanocolumn films containing more deep level defects give lower UV emission intensity. It is known that the intensity ratio of UV emission (I_{UV}) to deep level emission (I_{DLE}) is a suitable approach to estimate the optical quality of ZnO thin films [42]. The calculated relative integrated PL intensity ratio (I_{UV}/I_{DLE}) for all samples is given in Table 2. As seen in Table 2, that the intensity ratio increases as the annealing temperature increases to 500 °C, and then decreases when the temperature further increases up to 700 °C. Table 2 showed that the UV peak position of the ZnO thin films are blue-shifted from 383.5 to 381.5 nm with increase of the annealing temperature, which may be due to the increasing of grain size of ZnO thin films. As seen in Table 2, that FWHM of UV peak of the ZnO thin films decreased as the post-annealing temperature increased.

To study the effect of the post-annealing temperatures on the electrical properties of as-grown and annealed ZnO films, current–voltage measurements were performed by changing the bias voltage from −5 to +5 V at room temperature. Figure 4 reveals the typical I–V measurements of ZnO thin films grown on PS substrate; as-grown and annealed under the temperatures of 300, 500, and 700 °C. Figure 4 demonstrates that the current level increases as the annealing temperature increases to 500 °C, and then decreases when the temperature further increases up to 700 °C. The highest current of 5.006 mA (with the bias voltage of +5 V) was obtained at an annealing temperature of 500 °C that can be relative to the increase of grain size, resulting in the decrease in electron scattering in grain boundaries [43].

Table 2 Summarized data from PL spectra of ZnO thin films

Annealing temperature (°C)	UV peak (nm)	FWHM of UV peak (nm)	I_{UV}/I_{DLE}
As-grown	383.5	39	0.96
300	383.1	38	2.70
500	382.8	34	6.24
700	381.5	31	1.63

4 Conclusions

ZnO thin films were chemically grown on PS substrates at a low temperature. ZnO thin films were then annealed at 300, 500, and 700 °C for 20 min in N_2 atmosphere. The effect of the post-annealing temperature on the structural, optical, and electrical properties of ZnO thin films on PS substrates are investigated by X-ray diffraction, field emission scanning electron microscopy, and photoluminescence spectroscopy. The decrease of FWHM value and tensile strain (and increase of grain size) indicates that the increase of annealing temperature enhanced the crystal quality of fabricated ZnO thin films. The FESEM images demonstrated that the ZnO thin films are compact array ZnO nanocolumns and were perpendicularly grown to the PS substrate. The PL spectra indicate that the UV peak position of the ZnO thin films are blue-shifted from 383.5 to 381.5 nm with increase of the annealing temperature. Under the bias voltage of +5 V, the highest current of 5.006 mA was obtained at an annealing temperature of 500 °C.

Acknowledgments The author gratefully acknowledges the financial support of Babol University of Technology.

References

1. Z. Hosseini, A. Mortezaali, Sens. Actuators B Chem. **207**, 865–871 (2015)
2. K. Gurav, M. Gang, S. Shin, U. Patil, P. Deshmukh, G. Agawane, M. Suryawanshi, S. Pawar, P. Patil, C. Lokhande, Sens. Actuators B Chem. **190**, 439–445 (2014)
3. A. Echresh, C.O. Chey, M.Z. Shoushtari, O. Nur, M. Willander, J. Appl. Phys. **116**, 193104 (2014)
4. Z. Alaie, S.M. Nejad, M.H. Yousefi, J. Mater. Sci.: Mater. Electron. **25**, 852–856 (2014)
5. M. Thambidurai, N. Muthukumarasamy, D. Velauthapillai, C. Lee, Mater. Lett. **92**, 104–107 (2013)
6. I. Gonzalez-Valls, Y. Yu, B. Ballesteros, J. Oro, M. Lira-Cantu, J. Power Sources **196**, 6609–6621 (2011)
7. X.W. Sun, B. Ling, J.L. Zhao, S.T. Tan, Y. Yang, Y. Shen, Z.L. Dong, X. Li, Appl. Phys. Lett. **95**, 3124 (2009)
8. E. Makarona, M. Skoulikidou, T. Kyrasta, A. Smyrnakis, A. Zeniou, E. Gogolides, C. Tsamis, Mater. Lett. **142**, 211–216 (2015)
9. R. Ghosh, P. Giri, K. Imakita, M. Fujii, J. Alloys Compd. **638**, 419–428 (2015)
10. S. Chu, M. Olmedo, Z. Yang, J. Kong, J. Liu, Appl. Phys. Lett. **93**, 181106 (2008)
11. H. Zhang, X. Lv, C. Lv, Z. Jia, Opt. Eng. **51**, 099003-099001–099003-099005 (2012)
12. J.Y. Chen, K.W. Sun, Sol. Energy Mater. Sol. Cells **94**, 930–934 (2010)
13. İ. Polat, J. Mater. Sci.: Mater. Electron. **25**, 3721–3726 (2014)
14. D.-K. Kim, C.-B. Park, J. Mater. Sci.: Mater. Electron. **25**, 1589–1595 (2014)
15. J. Liang, H. Lai, Y. Chen, Appl. Surf. Sci. **256**, 7305–7310 (2010)
16. S.J. Kang, Y.H. Joung, Appl. Surf. Sci. **253**, 7330–7335 (2007)
17. J. Bian, X. Li, X. Gao, W. Yu, L. Chen, Appl. Phys. Lett. **84**, 541–543 (2004)
18. H.S. Kang, J.S. Kang, J.W. Kim, S.Y. Lee, J. Appl. Phys. **95**, 1246–1250 (2004)
19. L. Cui, G.-G. Wang, H.-Y. Zhang, R. Sun, X.-P. Kuang, J.-C. Han, Ceram. Int. **39**, 3261–3268 (2013)
20. L. Cui, H.-Y. Zhang, G.-G. Wang, F.-X. Yang, X.-P. Kuang, R. Sun, J.-C. Han, Appl. Surf. Sci. **258**, 2479–2485 (2012)
21. B. Zhu, X. Zhao, F. Su, G. Li, X. Wu, J. Wu, R. Wu, Vacuum **84**, 1280–1286 (2010)
22. K.G. Yim, M.S. Kim, S. Kim, J.-Y. Leem, G. Nam, S.M. Jeon, D.-Y. Lee, J.S. Kim, J.S. Kim, J.I. Lee, J. Korean Phys. Soc. **60**, 1605–1610 (2012)
23. J. Lim, K. Shin, H.W. Kim, C. Lee, J. Lumin. **109**, 181–185 (2004)
24. K.H. Yoon, J.-W. Choi, D.-H. Lee, Thin Solid Films **302**, 116–121 (1997)
25. X. Zhao, C. Kim, J. Lee, C. Shin, J. Heo, J. Leem, H. Ryu, J. Chang, H. Lee, C. Son, Appl. Surf. Sci. **255**, 5861–5865 (2009)
26. R. Hong, J. Huang, H. He, Z. Fan, J. Shao, Appl. Surf. Sci. **242**, 346–352 (2005)
27. C. Wang, P. Zhang, J. Yue, Y. Zhang, L. Zheng, Phys. B **403**, 2235–2240 (2008)
28. H. Lee, S. Lau, Y. Wang, B. Tay, H. Hng, Thin Solid Films **458**, 15–19 (2004)
29. G. Sanon, R. Rup, A. Mansingh, Thin Solid Films **190**, 287–301 (1990)
30. F. Lotgering, J. Inorg. Nucl. Chem. **9**, 113–123 (1959)
31. S. Gu, R. Zhang, J. Sun, L. Zhang, T. Kuech, Appl. Phys. Lett. **76**, 3454–3456 (2000)
32. W. Kwok, A.B. Djurišić, Y.H. Leung, D. Li, K. Tam, D. Phillips, W. Chan, Appl. Phys. Lett. **89**, 183112 (2006)
33. X. Wang, Z. Tian, T. Yu, H. Tian, J. Zhang, S. Yuan, X. Zhang, Z. Li, Z. Zou, Nanotechnology **21**, 065703 (2010)
34. S.H. Lee, H.J. Lee, H. Goto, M.w. Cho, T. Yao, Phys. Status Solidi (c) **4**, 1747–1750 (2007)
35. W. Park, Y. Jun, S. Jung, G.-C. Yi, Appl. Phys. Lett. **82**, 964–966 (2003)
36. B. Zhang, N. Binh, K. Wakatsuki, Y. Segawa, Y. Kashiwaba, K. Haga, Nanotechnology **15**, S382 (2004)
37. K. Vanheusden, W. Warren, C. Seager, D. Tallant, J. Voigt, B. Gnade, J. Appl. Phys. **79**, 7983–7990 (1996)
38. M. Liu, A. Kitai, P. Mascher, J. Lumin. **54**, 35–42 (1992)
39. J. Zhong, A.H. Kitai, P. Mascher, W. Puff, J. Electrochem. Soc. **140**, 3644–3649 (1993)
40. R. Dingle, Phys. Rev. Lett. **23**, 579 (1969)
41. L. Yang, Q. Zhao, M. Willander, J. Alloys Compd. **469**, 623–629 (2009)
42. C.-C. Lin, H.-P. Chen, H.-C. Liao, S.-Y. Chen, Appl. Phys. Lett. **86**, 183103 (2005)
43. J.-P. Lin, J.-M. Wu, Appl. Phys. Lett. **92**, 134103–134106 (2008)